

# Proteins at air-water and oil-water interfaces in an all-atom model

Yani Zhao and Marek Cieplak\*  
Institute of Physics, Polish Academy of Sciences,  
Al. Lotników 32/46, 02-668 Warsaw,  
Poland

(Dated: November 9, 2018)

We study the behavior of five proteins at the air-water and oil-water interfaces by all-atom molecular dynamics. The proteins are found to get distorted when pinned to the interface. This behavior is consistent with the phenomenological way of introducing the interfaces in a coarse-grained model through a force that depends on the hydrophathy indices of the residues. Proteins couple to the oil-water interface stronger than to the air-water one. They diffuse slower at the oil-water interface but do not depin from it, whereas depinning events are observed at the other interface. The reduction of the disulfide bonds slows the diffusion down.

## I. INTRODUCTION

Fluid-fluid interfaces, such as oil-water, air-water, and vapor-water systems, are fast changing and rough at the molecular time and length scales. Despite these transient features, the interfaces exhibit preferred orientations of the water molecules as evidenced by the surface vibrational sum frequency spectroscopy (VSFS)<sup>1,2</sup>. They have also been a subject of theoretical research. For instance, Sega and Dellago<sup>3</sup> have studied differences in the density profile and surface tension between seven models of the molecules of water near the air-water interface.

Proteins staying at the fluid-fluid interfaces add an additional complexity to this dynamics because of the variety of the chemical groups in the side chains that interact with molecules of the fluids in different manners. In bulk water, the folded chain of a globular protein is stabilized by hydrogen bonds and by interactions with the molecules of water. However, if there is a nearby interface, the protein may diffuse in its direction and get adsorbed. Polar and charged groups are then drawn into the bulk water, whereas the hydrocarbon groups seek the oil or vapor. As a result, the protein gets distorted and may lose its biological functionality<sup>4-6</sup>. Many proteins coming to the interface may form a viscoelastic film<sup>7-14</sup>. Understanding the behavior of protein films is important for the food industry, production of cosmetics, and physiology.

A theoretical description of such large dynamical systems requires making simplifications. In an approach proposed in ref.<sup>15</sup>, the protein at the air-water interface is described by a coarse-grained structure-based model<sup>16</sup>, the solvent is implicit, and the effect of the interface is introduced through a force that is coupled to the hydrophathy indices,  $q_i$ , associated with the amino acid residues. There are many hydrophathy scales<sup>17</sup> and the model makes use of the one proposed by Kyte and Doolittle<sup>18</sup>. In this scale, the values of  $q_i$  range between  $-4.5$  for the polar and charged ARG and  $4.5$  for the most hydrophobic ILE. The interface-related force acting on the  $i$ th  $\alpha$ -C atom is given by<sup>15</sup>

$$F_i^{wa} = q_i A \frac{\exp(-z_i^2/2W^2)}{\sqrt{2\pi}W} \quad (1)$$

where the amplitude  $A$  is set equal to  $10 \epsilon$ , and  $W=5 \text{ \AA}$ . Parameter  $W$  specifies the width of the interface and parameter  $A$  has been selected so that when a protein comes to the interface it does not depin from it. Smaller values of  $A$  allow for depinning of several proteins that have been studied<sup>15</sup>. Parameter  $A$  is given in terms of  $\epsilon$  which is equal to the depth of the potential in the effective contact interaction between two residues.  $\epsilon$  has been calibrated<sup>19</sup> to be of order  $110 \text{ pN \AA}$ .

This phenomenological model has been used to demonstrate glassy behavior of films made of lysozymes, protein G, and hydrophobin<sup>15</sup>. Subsequently, it was employed to study interface-induced topological changes in proteins<sup>20</sup>, such as tying and untying of a shallow knots in the proteins. Most recently, it was used to explain stabilization of beer foams by adsorption of the isoforms of the lipid transfer protein 1 (LTP1) to the surfaces of  $\text{CO}_2$  bubbles<sup>21</sup>.

Here, we focus on the atomic-level justification of the model – the subject that we started to discuss in the context of the beer proteins<sup>21</sup>. We perform all-atom simulations for five proteins: tryptophan cage (PDB:1L2Y), streptococcal protein G (PDB:1GB1), hydrophobin HFBI (PDB:2FZ6), LTP1 (PDB:1LIP), and the hen egg-white lysozyme (PDB:2LYZ). The sequential lengths of these proteins are correspondingly 20, 56, 72, 91 and 129. For brevity, we shall refer to the proteins by using their PDB structure codes. Three of these proteins, 1LIP, 2FZ6 and 2LYZ, are stabilized by  $n_{SS}$  disulfide bonds. For the three proteins,  $n_{SS}$  is equal to 4, but we also consider the reduced systems in which  $n_{SS}=0$ . We study single proteins and not films made of the proteins. The overall hydrophathy of a protein with the sequential length  $N$  can be characterized by the parameter  $H = 1/N \sum_{i=1}^N q_i$ . For the hydrophathy scale of Kyte and Doolittle, it is equal to  $-0.95$ ,  $-0.63$ ,  $+0.27$ ,  $-0.38$ , and  $-0.47$  for 1L2Y, 1GB1, 2FZ6,

1LIP and 2LYZ, respectively. Thus, only 2FZ6 (hydrophobin) is overall hydrophobic whereas the remaining proteins are overall hydrophilic. The reason to select these proteins is that they have already been studied within the coarse-grained model either in ref.<sup>15</sup> (1GB1, 2FZ6, and 2LYZ) or in ref.<sup>21</sup> (1LIP). 2LYZ is one of the proteins used in the experimental studies of thin films<sup>12</sup>.

The phenomenological model predicts that the air-water interface distorts proteins and leads to adjustment of their orientation to optimize the hydrophathy-related forces. Here, we demonstrate that the all-atom model acts in a similar fashion, but the proteins do not necessarily stay pinned at the interface. Permanent pinning at the air-water interface occurs for 1L2Y and 2FZ6, but not for the remaining proteins. In the latter case, we study multiple pinning events and determine their durations. Finally, we extend the studies to proteins at the oil-water interface. In this case, all of the proteins studied stay pinned there.

The formation of interface between two immiscible phases is a common phenomenon observed in ordinary everyday events (like beer foams<sup>21</sup>) as well as in biological processes. The understanding of the molecular processes at interfaces between liquids with different hydrophobicities is relevant to the biological activity of proteins in living organisms, and is important to the development of new systems through the tools of biotechnology. For example, the blood/biomaterial interfaces can be well mimicked by a hydrophobic/hydrophilic interfacial model<sup>22</sup>. The previous experimental work<sup>22</sup> has been exhibited that, proteins with hydrophobic surfaces possess fast adsorption rates at the air-water interface, while these with hydrophilic surfaces exhibit low affinity at the interface. Our simulating results coincide very well with the experimental observation, i. e. the affinity of 2FZ6 at the air-water interface is much higher than that of 1GB1.

## II. METHODS

The simulations are performed by using the NAMD<sup>23</sup> all-atom molecular dynamics package with the CHARMM22 force field<sup>24</sup>. The TIP3P water model<sup>25</sup> is used. The system is placed in a simulation box which extends between  $-L_x$  and  $L_x$  in the  $x$  and  $y$  directions, and  $-L_z$  and  $L_z$  along the  $z$ -direction. We take  $L_x=50$  Å and  $L_z$  is equal to 100 Å for the air-water interface and 50 Å for the oil-water one. In both cases, the water molecules are placed initially in the space corresponding to  $z \leq 0$ , and the interface is extended in the  $x-y$  plane. In order to make the water molecules prefer staying in the lower half of the box, we place a hydrophilic wall at the bottom of the air-water system (at  $z=-L_z$ ). The presence of the wall efficiently prevents the diffusion of water molecules to the air phase (with  $z > 0$ ) under the periodic boundary conditions, which are applied to all directions for both interfaces. However, this wall is not needed in the oil-water case. The immiscible nature of oil and water molecules generate an obvious interface between the two phases. The wall is composed of 6728 asparagines<sup>21</sup> that are arranged into a single layer. The  $\alpha$ -C atoms are anchored to the sites of the [001] face of an fcc lattice with the lattice constant of 5 Å. The side groups of the asparagines are directed into the box and they stay frozen during the simulations.

The major components of olive oil is oleic acid which constitutes 55 to 79% of the fluid<sup>26</sup>. The molecule is a chain of 18 carbon atoms (the length of the carbon-carbon bonds ranges from 1.31 to 1.53 Å) with the first one forming bonds with two oxygen atoms as illustrated in Fig. S1 in the Supplementary Information (SI). The density of oleic acid is 0.89 g/cm<sup>3</sup>.<sup>27</sup> To generate the oil-water interface, we place the oleic acid molecules initially in the upper half of the box.

It is difficult to perform full-scale all-atom simulation in which the protein is placed in the bulk water, gets equilibrated, and then diffuses to the interface. Such a simulation would require tremendous averaging necessitated, by the dynamic nature of the interface, evolution of the protein, and the motion of the water molecules in the bulk. Therefore, we perform a simplified calculation in which we just explore the effects of the interface on the protein. In the initial state, we place the protein right at the interface so that the center of mass of the protein is located at (0,0,0). The protein can have various orientations that can be characterized by the direction that the hydrophathy vector makes with the  $z$ -axis. The vector is defined<sup>15</sup> as  $\vec{h} = \frac{1}{N} \sum_{i=1}^N q_i \vec{\delta}_i$ .  $\vec{\delta}_i$  is the position vector of the  $i$ th residue with respect to the center of mass of the protein, and  $N$  is the total number of the residues. We have focused on two orientations: in orientation I the native  $\vec{h}$  points in the positive  $z$ -direction and in orientation II, in the opposite direction. Orientation I is expected to provide a preferred alignment.

To neutralize the charge of the protein, Na<sup>+</sup> or Cl<sup>-</sup> ions are added to the system. For example, four Na<sup>+</sup> ions, two Cl<sup>-</sup> ions, one Cl<sup>-</sup> ion and eight Cl<sup>-</sup> were required in the case of 1GB1, 1LIP, 1L2Y, and 2LYZ, respectively. For 2FZ6, no neutralizing ions are needed. The electrostatic interactions are accounted for by using the Particle Mesh Ewald method<sup>29</sup>.

In the next stage, the interfacial system is minimized for 0.02 ns by the conjugate gradient algorithm with all atoms being allowed to move. The minimization is performed at constant volume. The equilibration of the system is performed in two steps: 2 ns at  $T=150$  K and then  $\geq 10$  ns at 300 K. In both steps, the system is simulated in the canonical ensemble (NVT) with the Langevin temperature control. The timestep is 2 fs in our simulations. Each trajectory lasts for 50 ns for proteins 1L2Y and

1LIP at both air-water and oil-water cases. It lasts for 10 ns for other proteins.

The instantaneous orientation of the protein is characterized by a parameter  $\theta$ , which is the angle formed between the instantaneous hydrophathy vector  $\vec{h}$  and the positive  $z$ -axis.  $\theta$  is initially  $0^\circ$  and  $180^\circ$  for orientation I and II, respectively. We characterize location of the protein by the  $z$ -coordinate of its center of mass,  $z_{CM}$ , and the radial component of the center of mass in the  $x-y$  plane,  $r_{CM}$ . The geometry of proteins is described by the radius of gyration,  $R_g$ , and the vertical thickness,  $\Delta z = z_{\max, C_\alpha} - z_{\min, C_\alpha}$ , estimated based only on the  $\alpha-C$  atoms. In addition, we determine RMSD, the root-mean-square deviation from the native state, and parameter  $w$ , constructed from the three eigenvalues of the moment of inertia. This parameter distinguishes between the flat ( $w < 0$ ), elongated ( $w > 0$ ) and globular ( $w \approx 0$ ) shapes<sup>15</sup>.

### III. RESULTS

On relaxation, the interface becomes rough (some water molecules escape to the air, creating vapor) and we average the density field over 2 ns. Fig. 1 shows the number density profile of the water molecules along the  $z$ -axis (away from the wall at the bottom) and along the radial direction in the  $x-y$  plane. The number density of water in the bulk region is  $3.32 \pm 0.04 \times 10^{-2} / \text{\AA}^3$ , which is close to  $3.34 \times 10^{28} \text{ m}^{-3}$  for water under the normal conditions. We observe that  $\rho(z)$  goes down from the bulk value to zero at  $z = -5 \text{ \AA}$  and the width of the interface is about  $10 \text{ \AA}$ . The mid-point of the interface is at  $-12 \text{ \AA}$ . The bulk density of water is the same at both kinds of the interface. In the oil-water case,  $\rho(z)$  of water goes to zero at  $11 \text{ \AA}$  and the mid-point of the interface is at  $0 \text{ \AA}$ . The density of the oil molecules disappears at  $-7 \text{ \AA}$  and the corresponding mid-point is at  $3 \text{ \AA}$ . The width of the interface here can be defined as the separation between the  $z$  values at which water and oil reach their respective bulk densities. Such a width is about  $20 \text{ \AA}$ , which is twice as large as the width of the air-water interface.

Fig. 1 (the rightmost panels) also shows the average angle that the polarization vector of the water molecules makes with the  $x-y$  plane. We observe that, the polarization of the interfacial water molecules tends to stay parallel to the interface regardless of the nature of the interface.

#### A. Proteins at the air-water interface.

As an illustration, we first consider the short protein 1L2Y shown in Fig. 2 at four stages: the initial placement in orientation I, after the energy minimization, after 2 ns equilibration at  $T=150 \text{ K}$ , and in a snapshot obtained towards the end of the 10 ns evolution at  $300 \text{ K}$ . 1L2Y has three hydrophobic residues (shown in red) that are located in the helical segment at the N-terminus. These residues are seen to get pinned at the interface whereas the hydrophilic C-terminal segment moves in water fairly freely, resulting in sudden changes in the parameters pertaining to the shape, such as  $\Delta z$ .

The left panels of Fig. 3 show the time evolution of  $\theta$ ,  $z_{CM}$ ,  $\Delta z$ , and  $r_{CM}$  for 1L2Y at  $T=300 \text{ K}$  when the protein starts in orientation I. During the 50 ns of the evolution, 1L2Y is seen to stay at the interface (constant  $z_{CM}$ ) and merely diffusing in the  $x-y$  plane (as evidenced by the behavior of  $r_{CM}$ ). There are noticeable temporal changes in  $\Delta z$  signifying conformational transformations. For instance,  $\Delta z$  switches from  $7.2$  to  $11.7 \text{ \AA}$  at  $t \sim 17.5 \text{ ns}$ . The angle  $\theta$  is zero initially, but then it stays more or less fixed at about  $50^\circ$ . The fact that this angle is not 0 reflects two circumstances: 1) the protein gets deformed which changes the direction of  $\vec{h}$ , 2) the hydrophathy indices have not been derived by using the atomic force field. Nevertheless, the constancy of  $\theta$  signifies existence of a preferred orientation, similar to what is observed in the phenomenological model.

If one starts in orientation II (the top panels of Fig. 4), the protein is seen to first dunk into the water phase completely where it rotates under the influence of thermal fluctuations. Subsequently, it diffuses back to the interface, gets pinned there around  $1.4 \text{ ns}$ , and  $\theta$  comes close to the value obtained for orientation I.

A similar behavior is observed for the hydrophobic 2FZ6 (the bottom panels). There are no desorption events in orientation I irrespective of the number of the disulfide bonds. An example of a conformation of 2FZ6 obtained from one trajectory starting in orientation I is shown in Fig. S2 in SI. For orientation II, 2FZ6 gets repinned at  $7.1$  or  $10.1 \text{ ns}$ , depending on whether  $n_{SS}$  is 4 or 0 (the latter is beyond the scale of the figure). The reduction in  $n_{SS}$  appears to slow the rotation of the protein which delays adsorption to the interface.

The other three proteins, 1LIP, 1GB1 and 2LYZ, are overall hydrophilic, but unlike 1L2Y, their hydrophobic residues are distributed in a dispersed manner. These proteins can adsorb to the interface and then leave it multiply, as illustrated in Fig. 5 for 1LIP. The left panels are for  $n_{SS}=0$  and orientation II. Nine absorption events are seen. The first of them starts at the beginning

and it lasts for 6.34 ns (the time counts from the last equilibrated conformation obtained at 150 K). The protein then dips into the water phase for 0.3 ns and afterwards it gets pinned for 1.68 ns. The durations of the remaining adsorption events observed are: 0.06, 0.28, 0.88, 0.72, 0.20, 1.00 and 0.12 ns successively. Each adsorption event comes with its own type of deformation, as evidenced by the different corresponding values of  $\Delta z$ . The right panels of Fig. 5 are for  $n_{SS}=4$  and orientation I. In this case, we observe four adsorption events. They last for 2.4, 2.8, 4.6 and 14.3 ns successively. The statistics of the adsorption times are too small to assess but they suggest a uniform distribution except for the regime of the short lasting events which corresponds to a border-line behavior.

The pinning of 1LIP to the interface is usually driven by just one residue. In the left panels of Fig. 5, i.e. for  $n_{SS} = 0$ , it is ILE-90 in all nine events. One corresponding conformation is shown in Fig. 6. For  $n_{SS}=4$ , illustrated in Fig. 7, the protein is more compact and observe more variety. The left panel shows pinning by LEU-1, which is observed in 70% of the trajectories. The middle panel shows pinning by PRO-21 and the right panel – by ILE-90. We have also observed pinning by LEU-63. All of these residues are hydrophobic except for PRO which is moderately hydrophilic in the Kyte and Doolittle scale ( $q_i=-1.6$ ). However, in the CHARMM22 force-field, PRO appears to behave as a hydrophobic residue. The special character of PRO is discussed in ref.<sup>17</sup>. Various values of the measured hydrophobicity of PRO have been reported. In particular Table I in ref. <sup>17</sup> cites the value of 2.34.

Proteins 1GB1 and 2LYZ are more hydrophilic than 1LIP so they are expected to be able to leave the interface with a greater ease. Nevertheless, they do get pinned. Fig. S3 in SI shows an example of pinning by VAL-21 in 1GB1 (the left panels) and by PRO-70 in 2LYZ with  $n_{SS}=4$  (the right panels). If the trajectories were starting from orientation I, the pinning events lasted for 0.06 and 0.08 ns for 1GB1 and 2LYZ respectively (0.10 ns for 2LYZ if  $n_{SS}=0$ ). In 5 trajectories of 10 ns, we observe no return to the interface in either of the two proteins. However, if one uses the aligned crystal structure refers to the optimal surface orientation in the initial state (named orientation O), the average duration time at the interface at T=300 K is 6.2 ns for 1GB1 and 3.4 (5.5) ns for 2LYZ with  $n_{SS} = 4$  ( $n_{SS} = 0$ ). This indicates that, proper surface orientation plays a key role in the adsorption of proteins at the interface.

It should be noted that our results pertain to single proteins. Their depinning will be inhibited, but not eliminated, if it is a part of a dense film<sup>15</sup>.

## B. Proteins at the oil-water interface.

The oil-water interface is broader and rougher than the air-water one. As a result, pinning is driven not by single residues but by more extended regions containing hydrophobic residues and the tendency to stay at the interface is generally stronger. An example of pinning of 1L2Y is shown in the left panel of Fig. 8. In this example, the protein is seen to adhere to the interface along its length, but further evolution generates conformations which partially stretch away from the interface. The right-hand panels of Fig. 3 show the corresponding evolution of  $\theta$ ,  $z_{CM}$ ,  $\Delta z$  and  $r_{CM}$  that starts from orientation I. The angle  $\theta$  is close to the one at the air-water interface, but it displays bigger fluctuations. However, the variations in  $\Delta z$  are stronger. The plot of  $z_{CM}$  suggests that the protein dips down from the average location of the middle of the interface (as indicated by the arrow) but, in fact, it stays pinned to the interface because the interface itself exhibits a change in shape. Also protein 2FZ6 stays at the interface for  $n_{SS}$  of 4 and 0 (not shown), which is analogous to what we observed for the air-water case.

Snapshots of the pinned conformations of 1LIP are shown in Fig. 8. The left panel corresponds to  $n_{SS} = 4$  and the pinning occurs at residues 1–4 (LEU, ASN, CYS, GLY) and 40–47 (SER, SER, GLY, ASP, ARG, GLN, THR, VAL). The right panel is for  $n_{SS} = 0$  and the pinning involves regions 17–23 (VAL, GLN, GLY, GLY, PRO, GLY, PRO), 61–73 (LEU, ASN, LEU, ASN, ASN, ALA, ALA, SER, ILE, PRO, SER, LYS, CYS), and 82 to 85 (SER, PRO, ASP, ILE). Such extended pinning regions are not observed in the case of air-water interface. The difference in behavior stems from the fact that the air-water interface is better defined, and thus corresponding to a larger surface tension, than the intermixed oil-water interface. The larger surface tension means that the protein tends to minimize its exposure to the air.

Fig. 9 shows that this protein does not depin during the simulations for both considered values of  $n_{SS}$  indicating a stronger coupling to the interface compared to the air-water case.  $\Delta z$  undergoes somewhat larger fluctuations for  $n_{SS}=0$  than for  $n_{SS}=4$  and the protein with all disulfide bonds present stays deeper in water. Fig. S4 in SI demonstrates that the shape-related parameters  $R_g$ , RMSD and  $w$  of 1L2Y and 1LIP at the oil-water interface are similar to those at the air-water one. The same conclusion holds true for proteins 1GB1 and 2LYZ, i. e. they depin from the air-water interface, but not from the oil-water interface. These results suggest that, the strength of pinning a protein may vary significantly at different interfaces but its interfacial-related distortion is comparable. For example, the average RMSD of 1GB1 is 1.15 Å when it is adsorbed at the air-water interface, while it is 1.20 Å at the oil-water interface. The amplitude of the distortion in all-atom simulations is roughly 7 times smaller

than that presented in ref.<sup>15</sup> for the same protein (see Fig. 2 of ref.<sup>15</sup>). Nevertheless, one has to note that, the strength of the interface-related force is selected as  $A = 10 \epsilon$  in the coarse-grained model to prevent the depinning of proteins. The distortion of proteins can be reduced by decreasing the values of  $A$ . For instance, the average RMSD of 1GB1 at the interface decreases from 8.80 Å at  $A = 10 \epsilon$  to 7.30 Å at  $A = 5 \epsilon$ . Moreover, the possibility of depinning from the interface increases as  $A$  decreases in the coarse-grained model. Another primary characteristic of the distortion of proteins is  $\Delta z$ , its values obtained in the all-atom simulations agree with that in the coarse-grained model (see Fig. 13 of ref.<sup>21</sup> for 1LIP).

It is interesting to determine the two-dimensional diffusion coefficient  $D_2 = \frac{\langle \Delta \vec{r}^2 \rangle}{4\Delta t}$  of a protein at the interface. Here,  $\Delta \vec{r}$  is the displacement of the protein determined over each lag time  $\Delta t$ .  $D_2$  is determined in the asymptotic time regime. In the coarse-grained model<sup>15</sup>, and in the limit of a dilute protein film, one gets 0.0630 and 0.0245 Å<sup>2</sup>/τ for 1GB1 and 2LYZ respectively. The time scale,  $\tau$ , is of order 1 ns and the results were obtained by considering trajectories lasting for 150 000  $\tau$  and by averaging over many proteins when at the interface. The time scale of the all-atom simulation of 10 ns is too short to approach the necessary asymptotic behavior to obtain the saturation in the effective time-dependent  $D_2$ . We can only investigate the initial dependence of such a  $D_2$ . We measure  $\Delta \vec{r}$  every  $\Delta t = 0.02$  ns and averaged over 10 trajectories. Generally, we get the effective  $D_2$  to be substantially larger (typically by a factor of 50). Other than the short time scales (the lag time in the all-atom simulations is 0.02 ns but 1 ns in the coarse-grained model), the reason for the larger value is that in all-atom model, thermal fluctuations affect all heavy atoms, and not only the  $\alpha$ -C atoms.

For the oil-water interface, the short time values of  $D_2$  are  $11.74 \pm 0.6$ ,  $5.62 \pm 0.3$ ,  $5.14 \pm 0.3$ ,  $6.65 \pm 0.5$  and  $3.73 \pm 0.2$  Å<sup>2</sup>/ns for 1L2Y, 2FZ6 ( $n_{SS} = 4$ ), 1LIP ( $n_{SS} = 4$ ), 1GB1 and 2LYZ ( $n_{SS} = 4$ ), respectively. These results show that  $D_2$  depends primarily on the sequential length of the proteins: the longer the protein the slower the diffusion. For the air-water interface, we get  $D_2$  of  $27.74 \pm 1.8$  and  $10.54 \pm 0.4$  Å<sup>2</sup>/ns for 1L2Y and 2FZ6 ( $n_{SS} = 4$ ) respectively. Thus the diffusion at the air-water interface appears to be about twice as fast as at the oil-water one. This is because the oil phase anchors more hydrophobic residues. We also observe that the reduction of the disulfide bonds results in slowing the diffusion down. For instance, 2FZ6 with  $n_{SS} = 0$  has  $D_2$  of  $D = 9.77 \pm 0.2$  nm<sup>2</sup>/ns at the air-water interface, which is about 7% smaller than when  $n_{SS} = 4$ .

LTP1 has a post-translationally modified isoform LTP1b (PDB: 3GSH), which contains a fatty ligand ASY which stands for  $\alpha$ -ketol, 9-hydroxy-10-oxo-12(Z)-octadecenoic acid<sup>31</sup>. The C9 carbon of this ligand is covalently bound to the O2 atom of Asp-7 of the protein. The bonding site partitions the ligand ASY into two branches. The one from C10 to C18 is buried inside the cavity of LTP1b, while another branch from C1 to C8 lies on the surface of the protein and is hydrophobic. In the coarse-grained model<sup>21</sup>, the presence of the ligand contributes to a better adsorption of LTP1b to the air-water interface compared to LTP1<sup>21</sup> as ligand stretches out of the cavity.

In order to compare the behavior of the ligand at all-atom level to the coarse-grained model, we simulate LTP1b ( $n_{SS} = 4$ ) with orientation I at both the air-water and oil-water interfaces. The system is evolved at  $T = 300$  K for 10 ns. At the air-water interface, LTP1b can be adsorbed to the interface and then depinned multiple times just like LTP1. The branch of the ligand from C10 to C18 remains in the cavity throughout the simulation. The pinning of LTP1b can take place either at the C1 and C2 atoms of the ligand, as illustrated in the left panel of Fig. 10, or at PRO-21 of the protein. Both pinning centers are then exposed to the air. In the case of the oil-water interface, the buried branch of ligand still stays inside the cavity, but the exposed branch is fully in contact with the oil molecules, as shown in the right panel of Fig. 10. As a result, there is no depinning, highlighting the differences between the two interfaces.

#### IV. CONCLUSIONS

The differences in the behavior of proteins placed at the the air-water and oil-water interfaces have been attested experimentally by Sengupta and Damodaran<sup>32</sup>. They have found that the rates of adsorption of  $\beta$ -casein, BSA, and lysozyme to the oil-water interface were higher by an order of magnitude compared to the air-water interface. The oil used was triolein. They attributed the differences to the nature of the dispersive interactions at the interface: attractive in the case of oil and repulsive in the case of air.

Even though the two interfaces have different physical properties, the interfacial behavior of the five proteins studied here is fairly similar: there is a distortion and pinning. Thus the phenomenological coarse-grained model based on the hydropathy indices appears to capture the physics of pinning and distortion for both types of the interfaces. The model involves the amplitude of the hydropathy force and weakening of this amplitude can account for the depinning situations. However, some proteins are seen to depin and some do not, at least during the duration of the simulations. Thus the adjustment of the amplitude should be done on a case by case basis. In the oil-water case, our original amplitude  $A = 10 \epsilon$  would be then adequate in this respect.

It would be interesting to work out some rules that predict which hydrophilic proteins can depin and which can not. These rules should depend on the type of the interface. They should also reflect the observation that the hydrophobic residues appear to interact with the oil stronger than with the air (which, in our model, is represented simply by the absence of molecules). This effect can be captured by some strengthening of the Kyte and Doolittle<sup>18</sup> hydrophathy indices for the hydrophobic residues when dealing with oil.

These issues could perhaps be sorted out by considering artificial systems in which proteins are replaced by ligand-grafted nanoparticles as considered by Garbin et al.<sup>33</sup>. The ligand used in this case was amphiphilic mercapto-undecyl-tetra (ethylene glycol) and the experiment involved measurements of the surface pressure. One may consider grafting chains with homopeptidic tails to the nanoparticles to quantify interactions with the specific residues.

#### Acknowledgements

This research has been supported by the National Science Centre, Poland, under grant No. 2014/15/B/ST3/01905 and by the EU Joint Programme in Neurodegenerative Diseases project (JPND CD FP-688-059) through the National Science Centre (2014/15/Z/NZ1/00037) in Poland. The computer resources were supported by the PL-GRID infrastructure and financed by the European Regional Development Fund under the Operational Programme Innovative Economy NanoFun POIG.02.02.00-00-025/09.

- 
- \* Electronic address: mc@ifpan.edu.pl
- <sup>1</sup> Brown, M. G.; Walker, D. S.; Raymond, E. A.; Richmond, G. L. Vibrational sum-frequency spectroscopy of alkane/water interfaces: Experiment and theoretical simulation. *J. Phys. Chem. B* **2003**, *107*(1), 237-44.
  - <sup>2</sup> Moore, F. G.; Richmond, G. L. Integration or segregation: How do molecules behave at oil/water interfaces?. *Accounts of Chemical Research* **2008**, *41*(6), 739-48.
  - <sup>3</sup> Sega, M.; Dellago, C. Long-range dispersion effects on the water/vapor interface simulated using the most common models. *J. Phys. Chem. B* **2017**, *121*(15), 3798-3803.
  - <sup>4</sup> Adam, N. K. *The Physics and Chemistry of Surfaces*, Oxford University Press, London **1941**.
  - <sup>5</sup> Norde, W.; Giacomelli, C. E. BSA structural changes during homomolecular exchange between the adsorbed and the dissolved states. *J. Biotech.* **2000**, *79*, 259-268.
  - <sup>6</sup> Graham, D. E.; Phillips, M. C. Proteins at liquid interfaces: Kinetics of adsorption and surface denaturation. *J. Colloid Interface Sci.* **1979**, *70*, 403-414.
  - <sup>7</sup> Murray, B. S. Rheological properties of protein films. *Curr. Op. Colloid Interface Sci.* **2011**, *16*, 27-35.
  - <sup>8</sup> Cicuta, P. Compression and shear surface rheology in spread layers of beta-casein and beta-lactoglobulin. *J. Colloid Interface Sci.* **2007**, *308*, 93-9.
  - <sup>9</sup> Wierenga, P. A.; Kusters, H.; Egmond, M. R.; Voragen, A. G. J.; de Jongh, H. H. J. Importance of physical vs. chemical interactions in surface shear rheology. *Adv. Colloid Interface Sci.* **2006**, *119*, 131-9.
  - <sup>10</sup> Lee, M. H.; Reich, D. H.; Stebe, K.J.; Leheny, R. L. Combined passive and active microrheology study of protein-layer formation at an air-water interface. *Langmuir* **2010**, *26*, 2650-2658.
  - <sup>11</sup> Lee, M. H.; Cardinali, S. P.; Reich, D. H.; Stebe, K. J.; Leheny, R. L. Brownian dynamics of colloidal probes during protein-layer formation at an oil-water interface. *Soft Matt.* **2011**, *7*, 7635-7642.
  - <sup>12</sup> Allan, D. B.; Firester, D. M.; Allard, V. P.; Reich, D. H.; Stebe, K. J.; Leheny, R. L. Linear and nonlinear microrheology of lysozyme layers forming at the air-water interface. *Soft Matt.* **2014**, *10*, 7051-7060.
  - <sup>13</sup> Sollich, P.; Lequeux, F.; Hebraud, P.; Cates, M. E. Rheology of soft glassy materials. *Phys. Rev. Lett.* **1997**, *78*, 2020-2023.
  - <sup>14</sup> Malcolm, A. S.; Dexter, A. F.; Middelberg, A. P. J. Mechanical properties of interfacial films formed by lysozyme self-assembly at the air-water interface. *Langmuir* **2006**, *22*, 8897-8905.
  - <sup>15</sup> Cieplak, M.; Allen, D. B.; Leheny, R. L.; Reich, D. H. Proteins at air-water interfaces: a coarse-grained approach. *Langmuir* **2014**, *30*, 12888-96.
  - <sup>16</sup> Sułkowska, J. I.; Cieplak, M. Mechanical stretching of proteins a theoretical survey of the Protein Data Bank. *J. Phys.:Cond. Mat.* **2007**, *19*, 283201.
  - <sup>17</sup> Palliser, C. C.; Parry, D. A. D. Quantitative comparison of the ability of hydrophathy scales to recognize surface  $\beta$ -strands in proteins. *Proteins: Struct. Funct. Gen.* **2001**, *42*, 243-255.
  - <sup>18</sup> Kyte, J.; Doolittle, R. F. A simple method for displaying the hydrophatic character of a protein. *J. Mol. Biol.* **1982**, *157*, 105-32.
  - <sup>19</sup> Sikora, M., Sułkowska, J. I. & Cieplak, M. Mechanical strength of 17 134 model proteins and cysteine spliknots. *PLoS Comp. Biol.* **5**, e1000547 (2009).
  - <sup>20</sup> Zhao, Y.; Chwastyk, M.; Cieplak, M. Topological transformations in proteins: effects of heating and proximity of an interface. *Sci. Rep.* **2017**, *7*, 39851.
  - <sup>21</sup> Zhao, Y.; Cieplak, M. Structural changes in barley protein LTP1 isoforms at air-water interfaces. *Langmuir* **2017**, *33*(19), 4769-4780.
  - <sup>22</sup> Tripp, B. C.; Magda, J. J.; Andrade, J. D. Adsorption of globular proteins at the air/water interface as measured via dynamic surface tension: concentration dependence, mass-transfer considerations, and adsorption kinetics. *J. Colloid Interface Sci.* **1995**, *173*(1), 16-27.

- <sup>23</sup> Phillips, J. C.; Braun, R.; Wang, W.; Gumbart, J.; Tajkhorshid, E.; Villa, E.; Chipot, C.; Skeel, R. D.; Kale, L.; Schulten, K. Scalable molecular dynamics with NAMD. *J. Comp. Chem.* **2005**, *26*, 1781-1802.
- <sup>24</sup> MacKerell Jr, A. D.; Feig, M.; Brooks, C. L. III. Extending the treatment of backbone energetics in protein force fields: Limitations of gas-phase quantum mechanics in reproducing protein conformational distributions in molecular dynamics simulations. *J. Comp. Chem.* **2004**, *25*, 1400-1415.
- <sup>25</sup> Jorgensen, W. L.; Chandrasekhar, J.; Madura, J. D.; Impey, R. W.; Klein, M. L. Comparison of simple potential functions for simulating liquid water. *J. Chem. Phys.* **1983**, *79*(2), 926-35.
- <sup>26</sup> Ollivier, D.; Artaud, J.; Pinatel, C.; Durbec, J. P.; Guerere, M. Triacylglycerol and fatty acid compositions of French virgin olive oils. Characterization by chemometrics. *Journal of agricultural and food chemistry* **2003**, *51*(19), 5723-5731.
- <sup>27</sup> National Center for Biotechnology Information. PubChem Compound Database; CID=445639, <https://pubchem.ncbi.nlm.nih.gov/compound/445639>
- <sup>28</sup> Wołek, K.; Gómez-Sicilia, À.; Cieplak, M. Determination of contact maps in proteins: a combination of structural and chemical approaches. *J. Chem. Phys.* **2015**, *143*, 243105.
- <sup>29</sup> Darden, T. A.; York, D. M.; Pedersen, L. G. Particle Mesh Ewald: An Nlog(N) method for Ewald sums in large systems, *J. Chem. Phys.* **1993**, *15*, 10089.
- <sup>30</sup> Israelachvili, J.; Pashley, R. The hydrophobic interaction is long range, decaying exponentially with distance. *Nature* **1982**, *300*, 341-2.
- <sup>31</sup> Bakan, B.; Hamberg, M.; Larue, V.; Prange, T.; Marion, D.; Lascombe, M. B. The crystal structure of oxylipin-conjugated barley LTP1 highlights the unique plasticity of the hydrophobic cavity of these plant lipid-binding proteins. *Biochem. Biophys. Res. Commun.* **2009**, *390*(3), 780-785.
- <sup>32</sup> Sengupta T.; Damodaran, S. Role of dispersion interactions in the adsorption of proteins at oil-water and air-water interfaces. *Langmuir* **1998**, *14*, 6457-6469.
- <sup>33</sup> Garbin, V.; Jenkins, I.; Sinno, T.; Crocker, J. C.; Stebe, K. J. Interactions and stress relaxation in monolayers of soft nanoparticles at fluid-fluid interfaces. *Phys. Rev. Lett.* **2015**, *114*, 108301.

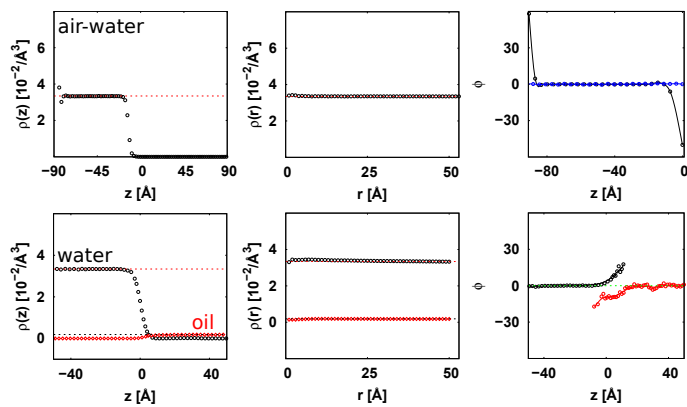


FIG. 1: The top panels: The number density profiles of water molecules at the air-water system along  $z$ -axis and the radial direction in the  $x - y$  plane. The red dashed line indicates the level characterizing water under atmospheric pressure in the plots of  $\rho(z)$  and  $\rho(r)$ . The bottom panels: similar to the top panels but for the oil-water interface. The red data points show results for the oil molecules.

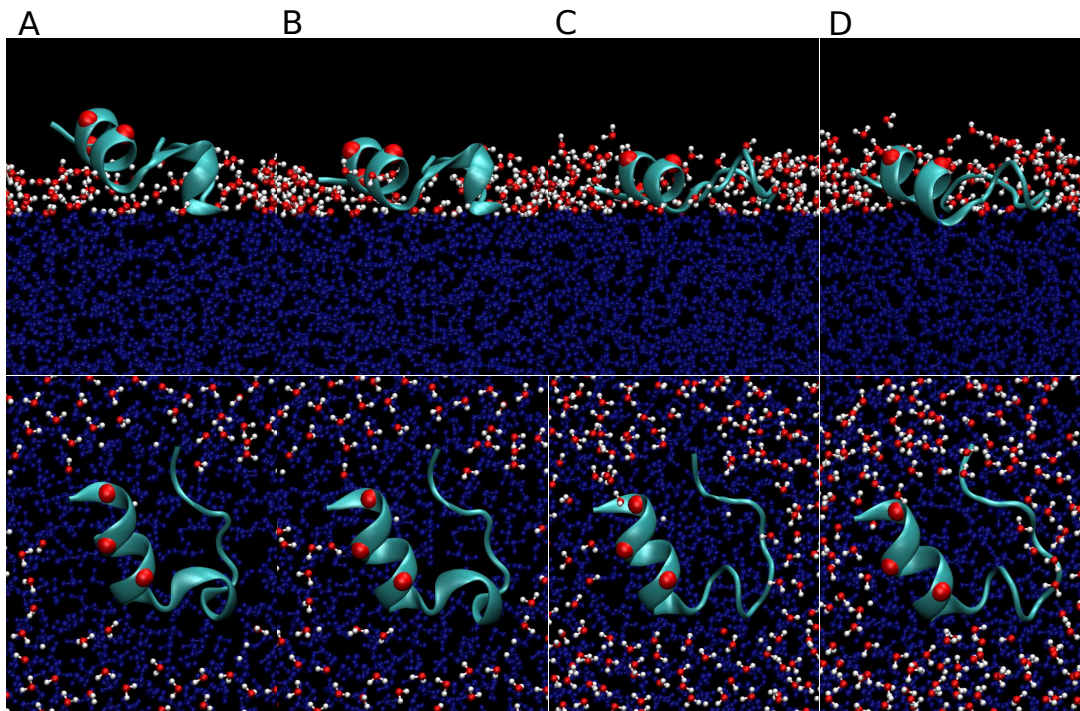


FIG. 2: Snapshots of protein 1L2Y placed in orientation I. The top panels correspond to the side view, and the bottom panels to the top view. The molecules of water at the interface, with  $z > -12$   $\text{\AA}$ , are shown in red and white and those in the bulk – in blue. A: The initial state of the system. B: The state after minimization. C: The state after 2 ns equilibration at  $T = 150$  K. D: A state at the end of the 10 ns time evolution at  $T = 300$  K.

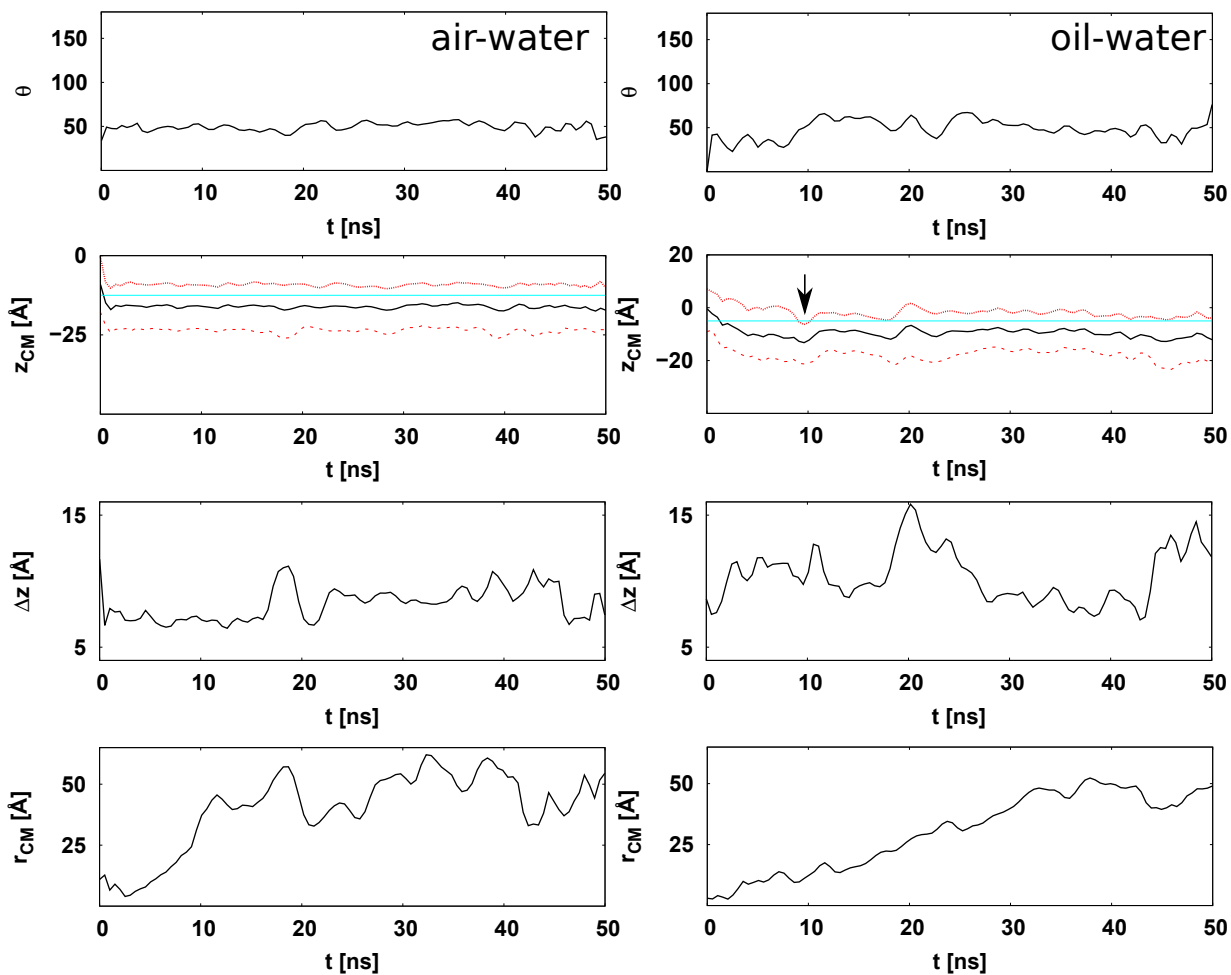


FIG. 3: Time evolution of  $\theta$ ,  $z_{CM}$ ,  $\Delta z$  and  $r_{CM}$  of 1L2Y starting in orientation I at the air-water (left) and oil-water (right) interfaces at  $T=300$  K. In the plot of  $z_{CM}$ , the black line shows the values of  $z_{CM}$ , the cyan line displays the average position of the interface, the red lines above and below the line corresponding to the interface indicate the vertical position of the top and bottom atoms of the protein. The arrow in the second panel on the right indicates a situation in which the protein is pinned at the interface but the interface itself is below its average position (see the left panel of Fig. 8).

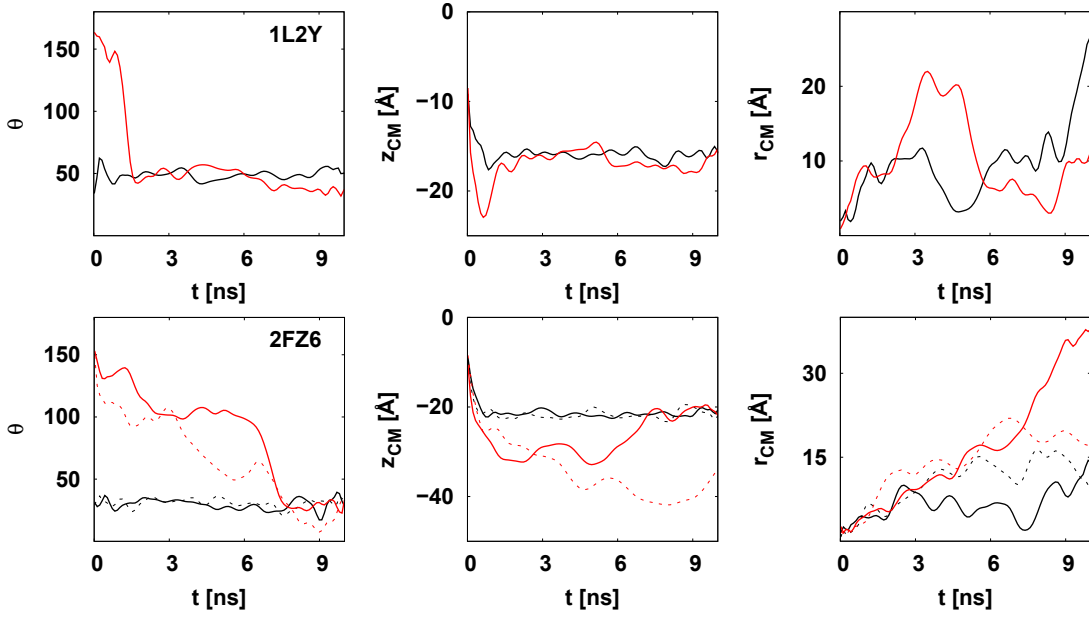


FIG. 4: Time evolution of  $\theta$ ,  $z_{CM}$  and  $r_{CM}$  for 1L2Y (the top panels) and 2FZ6 (the bottom panels) at the air-water interface. The black lines are for the starting orientation I and the red lines are for orientation II. For 2FZ6, the solid lines are for  $n_{SS} = 4$ , while the dashed line are for  $n_{SS} = 0$ .

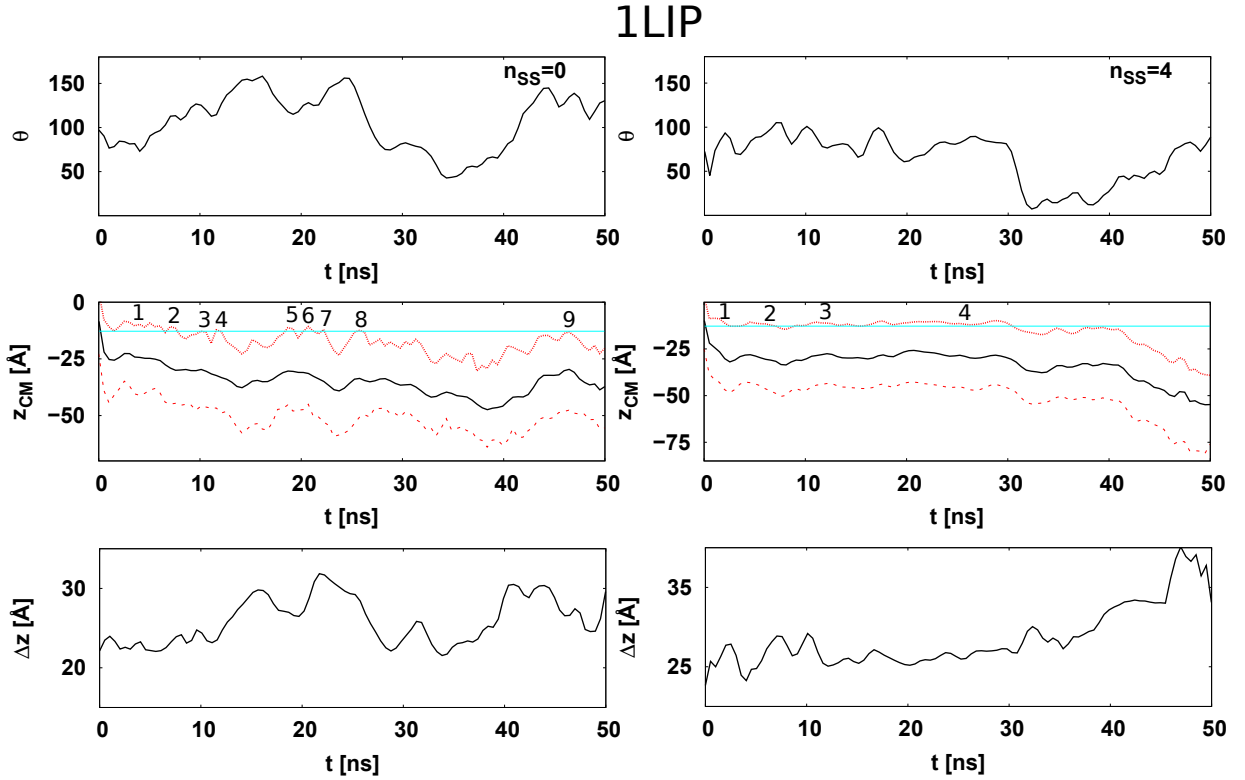


FIG. 5: Time evolution of  $\theta$ ,  $z_{CM}$  and  $\Delta z$  of 1LIP at  $n_{SS} = 0$  (left) in orientation II and  $n_{SS} = 4$  (right) in orientation I at the air-water interface. In the plot of  $z_{CM}$ , the black line shows the values of  $z_{CM}$ , the cyan line displays the average position of the air-water interface, the red lines above and below the interface are the top and bottom atoms of the protein along  $z$ -axis.

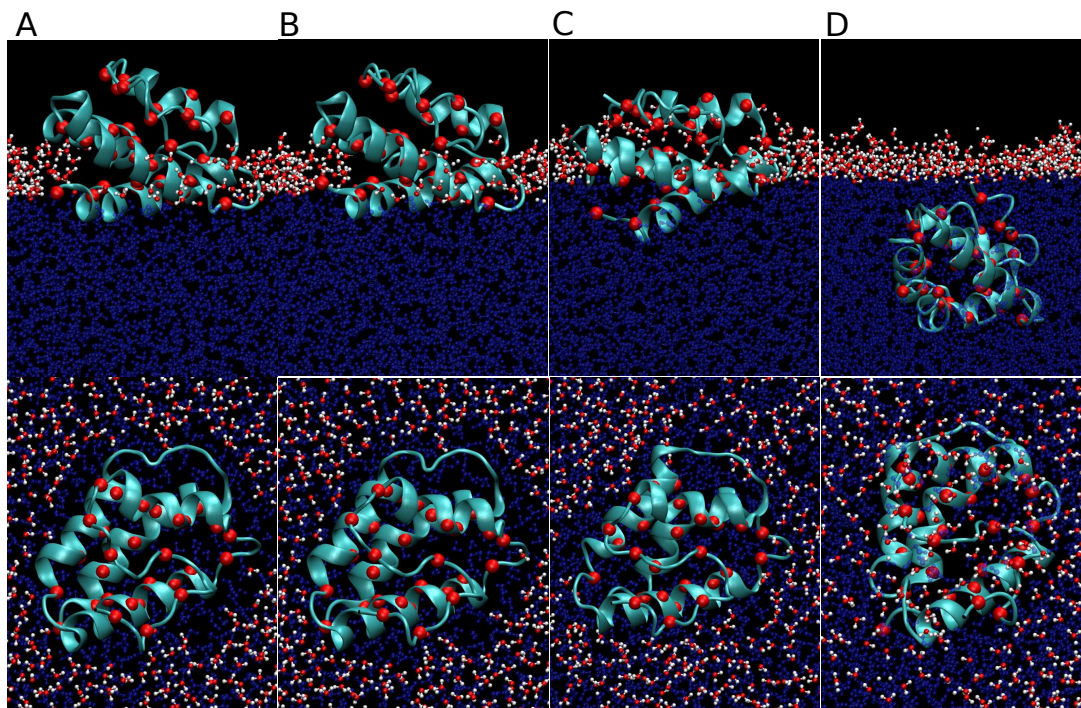


FIG. 6: Protein 1LIP with  $n_{SS} = 0$  initially placed in orientation II. A: The initial state of the system. B: The state after the energy minimization. C: The state after 2 ns equilibration at  $T = 150$  K. D: The final state of the system after 10 ns equilibration at  $T = 300$  K. The top panels show the side view, and the bottom panels – the top view.

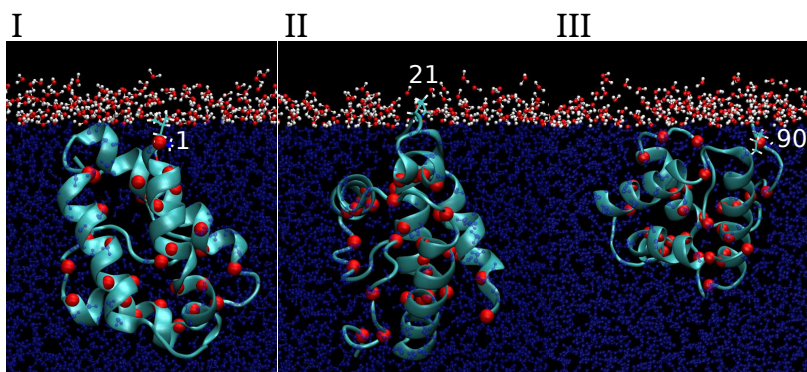


FIG. 7: Examples of conformations of 1LIP adsorbed at the air-water interface. In panels I through III, pinning is initiated by ILE-1 (for  $n_{SS}=4$ ), PRO-21 (for  $n_{SS}=0$ ), and ILE-90 (for  $n_{SS}=0$ ) respectively.

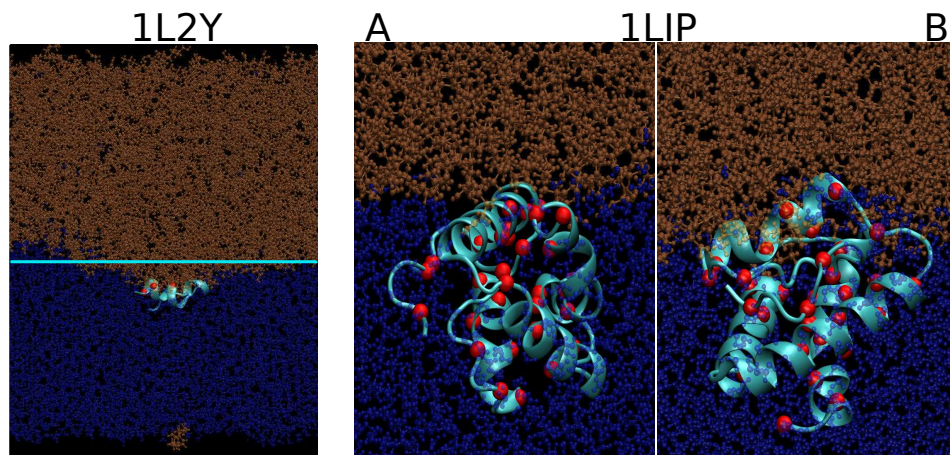


FIG. 8: Left: A snapshot of 1L2Y adsorbed at the oil-water interface. The cyan line indicates the average position of the interface. The molecules of oil are shown in orange. Right: 1LIP adsorbed at the oil-water interface at  $T = 300$  K. A: 1LIP with  $n_{SS} = 4$  after starting in orientation I. B: 1LIP with  $n_{SS} = 0$  after starting in orientation II.

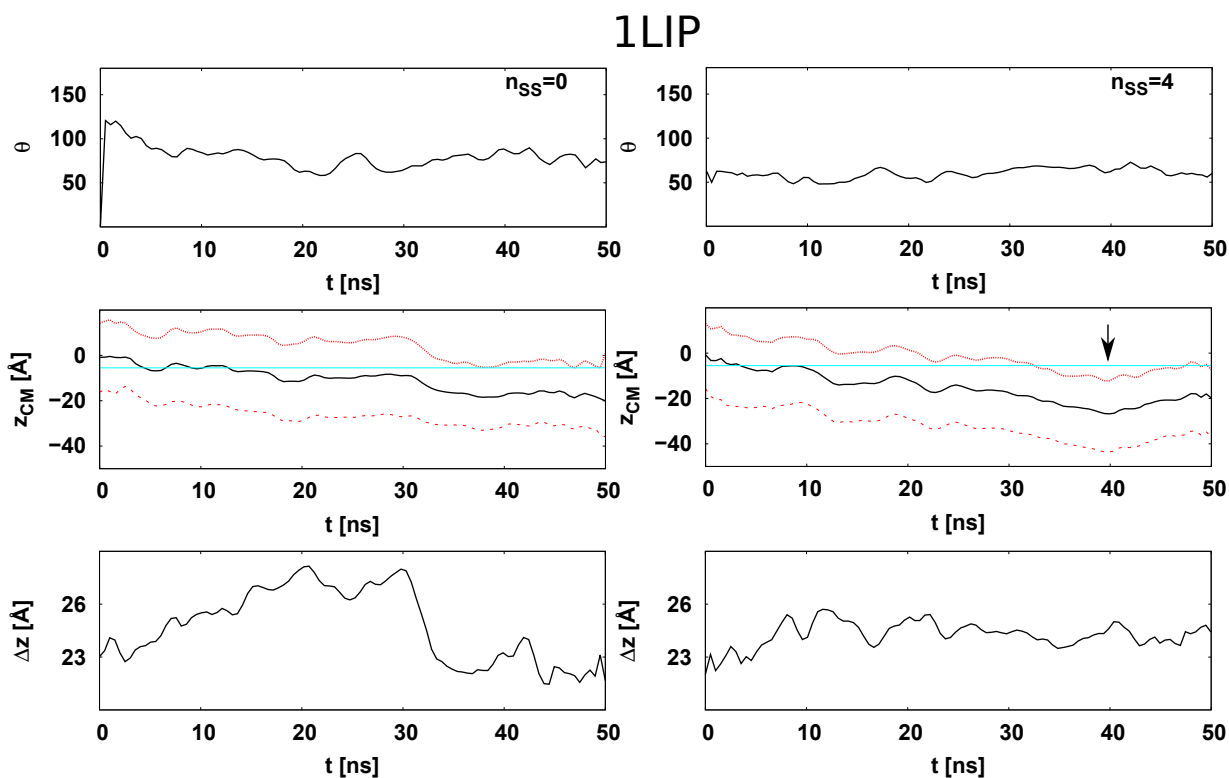


FIG. 9: Similar to Fig. 5, but for the oil-water interface.

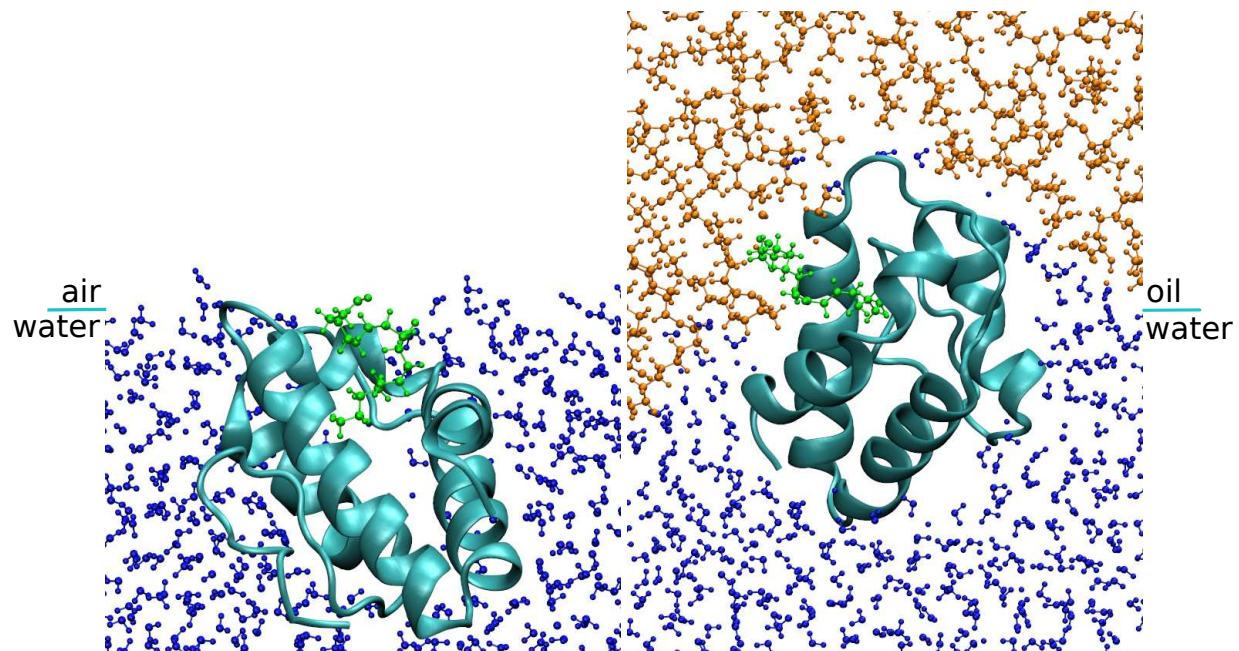


FIG. 10: Side view of LTP1b at the air-water (left panel) and oil-water (right panel) interfaces. The atoms of the ligand are shown in green. The water molecules are in blue and those of oil in orange.